

Drift- and Parameter-Compensated Flux Estimator for Persistent Zero-Stator-Frequency Operation of Sensorless-Controlled Induction Motors

Joachim Holtz, *Fellow, IEEE*, and Juntao Quan

Abstract—The performance of sensorless-controlled induction motors is poor at very low speed. The reasons are the limited accuracy of stator voltage acquisition and the presence of offset and drift components in the acquired signals.

To overcome these problems, a pure integrator is employed for stator flux estimation. The time-variable dc offset voltage is estimated from the flux drift in a parallel stator model and used to eliminate the offset by feedforward control. Residual high-frequency disturbances are compensated by feedback flux amplitude control. A linearization of the pulsewidth-modulation inverter transfer function and an improved stator resistance estimation scheme further enhance the system performance.

Experiments demonstrate high dynamic performance of sensorless control at extreme low speed and zero stator frequency.

Index Terms—Control at zero stator frequency, dc offset estimation, induction motor, pulsewidth-modulation (PWM) inverter model, sensorless speed control, stator flux estimator, stator resistance estimation.

I. INTRODUCTION

VECTOR-CONTROLLED induction motor drives without speed sensor have become an attractive and commercially expanding technology in the past few years [1]. The absence of the mechanical speed sensor reduces the cost and the volume of the drive motor. It does away with the sensor cable, and increases the reliability of the overall system. It is still a problem, though, to achieve robust sensorless control at very low speed, particularly in a region at and around zero stator frequency. The physical reason is that all estimation methods, directly or indirectly, rely on the effect of the rotor induced voltage, which becomes very small as the stator frequency reduces, and vanishes at zero stator frequency.

It has been the subject of recent research to narrow or eliminate the region of inoperability around zero stator frequency. One way toward this goal exploits spatial machine anisotropies that indicate either the actual rotor position, or the field angle [2]. It requires subjecting the machine to transient conditions so as to enable the identification of the anisotropic characteristics.

This can be done by injecting a continuous high-frequency signal into the stator winding [3], [4], or by exploiting the repetitive transient excitation caused by the switching of the pulsewidth-modulation (PWM) inverter [5]. These methods could solve the zero-frequency problem in principle, but not without incurring penalties. These are the requirement of additional hardware for signal acquisition, and/or the high computational load.

Under these circumstances is the restriction of using the fundamental model of the induction machine extremely attractive. This model considers only the fundamental spatial distributions of the flux density and the current density waves, thus describing the electromagnetic subsystem of the machine as a dynamic system of second order if complex state variables are used [6]. The approach tends to be inaccurate at lower stator frequency as the fundamental voltages are then low in magnitude. Their fundamental components are difficult to separate from the switching harmonics, and from the offset and noise components that act as disturbances in the signal acquisition process.

Recent research has aimed at improving the estimation accuracy of the fundamental model for flux estimation. The key quantity here is the phase angle of flux linkage vector, also referred to as the field angle δ . The field angle enables the transformation of the stator current vector into field coordinates, thus making the electromagnetic torque and the flux of the machine independently controllable. This is a prerequisite for maintaining the stability of a dynamic ac drive at any speed. Either the stator flux linkage vector or the rotor flux linkage vector can be used to define a field-oriented coordinate system. Preference is given here to stator field orientation which is simpler to implement.

II. LIMITS OF STABLE OPERATION AT LOW SPEED

In a sensorless drive system, the field angle, and also the mechanical speed, are estimated using the stator current vector and the stator voltage vector as input variables. Their accurate acquisition is a major concern for stable operation at very low speed.

A. Inverter Nonlinearity

The direct measurement of the stator voltages at the machine terminals is most accurate [7], but hardware requirements are quite substantial. The switched stator voltage waveforms require a large signal acquisition bandwidth, and electric isolation must

Paper IPCSD 03-043, presented at the 2002 Industry Applications Society Annual Meeting, Pittsburgh, PA, October 13-18, and approved for publication in the IEEE TRANSACTIONS ON INDUSTRY APPLICATIONS by the Industrial Drives Committee of the IEEE Industry Applications Society. Manuscript submitted for review July 1, 2002 and released for publication April 16, 2003.

J. Holtz is with the Electrical Machines and Drives Group, University of Wuppertal, 42097 Wuppertal, Germany (e-mail: j.holtz@ieee.org).

J. Quan was with Danaher Motion GmbH and Company KG, 40489 Dueseldorf, Germany. He is now with Rockwell Automation AG, CH-6036 Luzern, Switzerland (e-mail: juntao_quan@web.de).

Digital Object Identifier 10.1109/TIA.2003.813726

be maintained between the power circuit and the electronic control system. However, the processing of the analog signals introduces errors and offset. **Using the reference voltage of the pulsewidth modulator avoids all these problems.** This signal is readily available in the control unit, and it is free from harmonic components. **It does not exactly represent the stator voltages,** though, as distortions are introduced by the dead-time effect which cannot be completely eliminated even by the most sophisticated compensation strategies. Also, the PWM inverter itself exhibits nonlinear characteristics. It is the threshold voltages of the power devices that cause distortions of the machine voltages, and their effect is particularly pronounced at low speed when the fundamental voltage is low. The distortion components depend on the directions of the phase currents; their impact on the quality of current control and their compensation by a time displacement of the inverter control signals was described by Choi *et al.* [8]. Estimating the stator voltage vector for the purpose of state estimation requires modeling of the inverter nonlinearities. This reconstructs the true stator voltage vector \mathbf{u}_s from the inverter control signal \mathbf{u}^* [9]. An adaptive compensation scheme for the inverter nonlinearity is reported in [10].

B. Current Acquisition Errors

Also, the measured current signals can be in error due to unbalanced gains of the measurement channels, as well as from dc offset and drift. These disturbances have their origin in the analog portion of the current acquisition channels. They cause fluctuations of the machine torque, **generating speed oscillations of fundamental and double fundamental frequency** [9]. Chung *et al.* propose their compensation by closed-loop control on the basis of the resulting speed oscillations. This method requires precise speed measurement which cannot be substituted by speed estimation techniques. Moreover, the accuracy is poor under transient conditions and, hence, **residual errors** may persist.

C. Field Angle Estimation

DC offset and thermal drift have been ever since identified as major problems to accurate flux angle estimation at very low speed. A most common solution is the replacement of the stator flux integrator by a low-pass filter. The limited dc gain of such low-pass filter eases this problem as long as the stator frequency is much greater than the filter cutoff frequency. The phase angle difference between the integrator and the low-pass filter determines the field angle error. The lower limit of stable operation is at about five times the cutoff frequency and, thus, intolerably high. A simple way of lowering this boundary is limiting the peak values in stator coordinates of the estimated stator flux components to the flux reference magnitude [12]. While such limiting eliminates the dc offset from the flux signal, it introduces phase angle distortions in turn. The limit of stable operation is around a stator frequency of 2–3 Hz.

A more refined way of maintaining the stator flux vector close to its intended circular trajectory consists in not only clipping the peak amplitudes of its orthogonal components, but exerting a continuous influence on the flux vector magnitude. Hu and Wu [13] propose an adjustment of the estimated flux vector by closed-loop proportional-plus-integral (PI) control, forcing

the stator flux vector angle to lag the vector \mathbf{u}_i of the induced voltage by $\pi/2$. Although this would be the correct solution in principle, the magnitude of the induced voltage becomes extremely small at very low speed, which makes dc offset and other disturbances the dominant signals. Another major drawback of this method is the dynamic delay of the closed-loop control used for error correction. This delay generates dynamic errors at transient conditions. Possibly for this reason have the authors applied their methods only for flux monitoring, but not for field-oriented control in a closed loop.

Kubota *et al.* propose to estimate the dc offset using a full-order observer [7]. They exploit the fact that oscillations in speed and rotor flux magnitude occur in the presence of dc offset. The approach is highly computational. It requires computing the average values within a fundamental period of the estimated rotor flux components in stationary coordinates. These values are subsequently multiplied by coefficients derived from the system matrix, which in turn depend on the estimated speed. The results are summed up to yield increments of the estimated offset voltage components.

Also, Rodic *et al.* [14] use the deviations of the estimated rotor flux magnitude from its reference value to build a nonlinear flux observer. This observer is constructed as a second-order low-pass filter at low stator frequency; it converts to a first-order low-pass filter at higher stator frequency. The experimental results obtained with this method demonstrate moderate performance.

D. Stator Resistance Estimation

A further source of error in the estimation of the stator flux angle is the misalignment of the estimated stator resistance with its real value in the machine. The load dependent variations of the winding temperature may lead to up to $\pm 50\%$ error of the modeled stator resistance. Hence, the stator resistance must be continuously adapted to its correct value during operation. Ha and Lee [15] propose an identification scheme which relies on the computed difference between the real power input to the stator windings and the air-gap power, considering the actual load condition as calculated from the instantaneous reactive power, the stator current magnitude, and the stator frequency. Being obtained as a small difference between large quantities, the estimated stator resistance value tends to be inaccurate.

Mir *et al.* report on a stator resistance estimation scheme implemented in a direct torque control system [16]. The controlling variables are the stator flux magnitude and the electromagnetic torque. Any given combination of these variables defines a certain value of the stator current magnitude. A deviation of the measured current magnitude from this value is attributed to a change in stator resistance. The modeled value is then adjusted until the two currents coincide. It is apparent, though, from the experimental results that the estimation of the stator resistance is fairly inaccurate.

The approach of Guidi *et al.* [17] requires modeling the induction machine by a full-order observer. A misalignment of the modeled stator resistance is detected from a comparison between the measured and the estimated stator current vector. Introducing a linear displacement of the estimated stator current vector increases the sensitivity of the algorithm, provided

the displacement is adequately chosen. The experimental results look promising but might require improved disturbance rejection.

E. Overview

As a contribution to the aforementioned topics, this paper describes the design concept of a ready-to-implement sensorless drive control system for high performance at very low speed, including zero-stator-frequency operation. The system comprises a nonlinear inverter model for the estimation of the stator voltage vector, a precise dc offset estimator, a stator resistance adaptation scheme, and a fast compensator for residual disturbances like current gain unbalance, the current zero-crossing effect, and general model inaccuracies. The exact compensation of all these adverse effects permits using a pure integrator for stator flux estimation and, thus, provides long-term stability at zero-stator-frequency operation.

III. MODELING THE DRIVE SYSTEM COMPONENTS

A. Stator Flux Estimation

Among the various ways of establishing a machine model in terms of fundamental variables, preference is given for reasons of simplicity to the stator model. It is derived from the stator voltage equation in stator coordinates

$$\mathbf{u}_s = r_s \mathbf{i}_s + \frac{d\boldsymbol{\psi}_s}{d\tau} \quad (1)$$

where \mathbf{u}_s and \mathbf{i}_s are the space vectors representing the stator voltages and the stator currents, respectively, $\boldsymbol{\psi}_s$ is the stator flux linkage vector, and r_s is the stator resistance. Time is normalized as $\tau = \omega_{sR} t$, where ω_{sR} is the nominal stator frequency [6].

Equation (1) serves to estimate the stator flux linkage vector

$$\hat{\boldsymbol{\psi}}_s = \int (\hat{\mathbf{u}}_s - \hat{r}_s \hat{\mathbf{i}}_s) d\tau \quad (2)$$

from the measured or estimated variables

$$\hat{\mathbf{u}}_s = \mathbf{u}_s + \mathbf{u}_z \quad (3a)$$

$$\hat{\mathbf{i}}_s = \mathbf{i}_s + \mathbf{i}_z \quad (3b)$$

$$\hat{r}_s = r_s + \Delta r_s \quad (3c)$$

where \mathbf{u}_z and \mathbf{i}_z are space vectors representing the respective disturbances of the stator voltage and the stator current vector, Δr_s is the modeling error of the stator resistance, and $\hat{\cdot}$ marks a variable as estimated.

The signal content of the stator voltage disturbance vector \mathbf{u}_z in (3) is attributed to:

- the nonlinear characteristics of the PWM inverter;
- the ill-defined state of the inverter at current zero crossing;
- time and amplitude discretization errors of the pulsewidth modulator;
- errors due to incomplete dead-time compensation.

The disturbance vector \mathbf{i}_z superimposed to the stator current vector represents:

- dc offset and drift;
- gain unbalance of the current acquisition channels;
- current discretization errors;

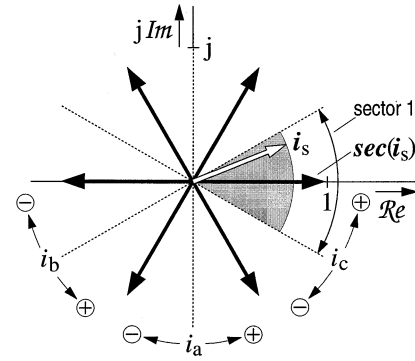


Fig. 1. The six possible discrete locations of the sector indicator $\sec(\mathbf{i}_s)$; the dotted lines mark the transitions at which the signs of the respective phase currents change.

- residual switching harmonics of the fundamental current signals.

Apart from the induction motor, represented by its fundamental model, only the imperfections of the PWM inverter, the dc offset, and the stator resistance will be reproduced here by models or estimators. The remaining disturbances consist of low-amplitude high-frequency signals which enables their elimination without employing specific models.

B. Nonlinear Inverter Model

The forward voltage of the power semiconductors can be approximated by a fixed-threshold voltage u_{th} and a current-dependent component $r_d i$, where r_d is the differential resistance and i is the forward current of the device. The resistive portion $r_d i$ of the inverter voltage is a linear function of the device current. The constant threshold voltage produces nonlinear voltage distortions. These can be higher in amplitude than the fundamental machine voltage at very low frequency.

The details of a nonlinear inverter model are described in [9]. It is demonstrated there that the effect of the threshold voltage in a particular bridge arm depends on the direction of the respective phase current, since a conducting device is always forward biased. The threshold voltage component of phase a is, therefore, $u_{th} \cdot \text{sign}(i_a)$. Making use of the definition of a voltage space vector by its three-phase voltage components [6] permits defining the threshold voltage vector

$$\mathbf{u}_{th} = \frac{2}{3} (u_{th} \text{sign}(i_a) + a u_{th} \text{sign}(i_b) + a^2 u_{th} \text{sign}(i_c)) \quad (4)$$

where $a = \exp(j2\pi/3)$ is the unity vector rotator.

Equation (4) can be rewritten as

$$\mathbf{u}_{th} = \frac{4}{3} u_{th} \cdot \sec(\mathbf{i}_s) \quad (5)$$

where the sector indicator

$$\sec(\mathbf{i}_s) = \frac{1}{2} (\text{sign}(i_a) + a \text{sign}(i_b) + a^2 \text{sign}(i_c)) \quad (6)$$

is a unity vector that marks the 60° sector in which the current space vector resides. The six discrete locations of the sector indicator are shown in Fig. 1. The argument of this unity vector is a kind of modulo $(\pi/3)$ function of the current space vector phase angle.

Fig. 2 shows the distortions that the inverter nonlinearity imposes on the stator voltage vector when the reference voltage

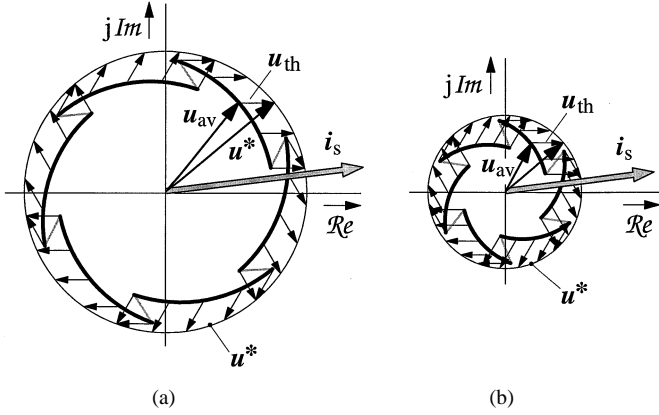


Fig. 2. The effect of inverter nonlinearity at two different values of stator frequency. The discontinuous trajectories \mathbf{u}_{av} represent the average stator voltage within a switching subcycle. (a) At $\omega_s = 0.017$. (b) At $\omega_s = 0.01$.

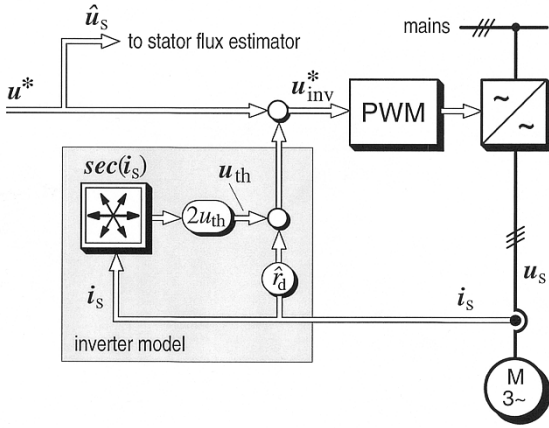


Fig. 3. Signal flow graph of a sensorless drive with compensation of the inverter nonlinearity.

vector is controlled to follow a circular trajectory. At the machine terminals, the average stator voltage per modulation cycle \mathbf{u}_{av} is discontinuous and exhibits strong sixth harmonic components. It has less fundamental content at motoring and more at regeneration [9].

Neglecting the switching harmonics, the transfer characteristics of the PWM inverter are

$$\mathbf{u}_s = \mathbf{u}_{inv}^* - \mathbf{u}_{th}(\mathbf{i}_s) - r_d \mathbf{i}_s. \quad (7)$$

The last two terms in (7) define the contributions of the nonlinear inverter model. With reversed signs, this model is inserted between the reference voltage vector and the pulsewidth modulator input to establish a linear relationship between \mathbf{u}^* and \mathbf{u}_s . The signal flow graph of Fig. 3 illustrates this.

The inverter model is characterized by two parameters, u_{th} and r_d . A method to identify the threshold voltage u_{th} is proposed in [9]. Ways of adapting u_{th} to the prevailing operating conditions are described in [10]. Such adaptation may be too much refinement for some applications.

The second parameter of the inverter model of Fig. 3 is the differential resistance r_d of the power devices. This resistance is identified as part of the estimation scheme described in Section III-E.

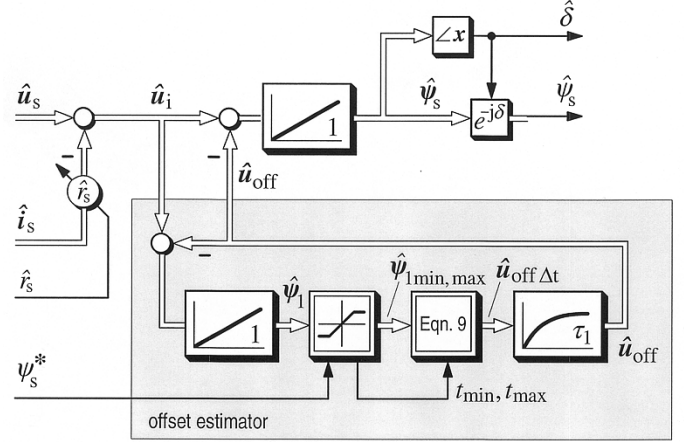


Fig. 4. Signal flow graph showing an offset voltage estimator for high-bandwidth stator flux estimation using a pure integrator.

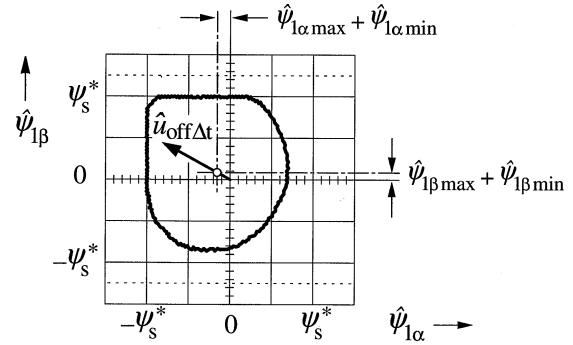


Fig. 5. Measured trajectory of the vector $\hat{\psi}_1$ showing the effect of uncompensated offset.

C. Offset Vector Estimation

According to (2), even minor dc components in the voltage and current signals accumulate in the process of integration to form a large offset in the estimated stator flux linkage vector. A solution to this problem exploits the fact that the offset vector is almost unidirectional while the derivative vector of the circular displacement rotates. The signal flow diagram of Fig. 4 shows the elements of an offset voltage estimator highlighted by a shaded frame. The induced voltage

$$\hat{\mathbf{u}}_i = \hat{\mathbf{u}}_s - \hat{r}_s \hat{\mathbf{i}}_s \quad (8)$$

serves as an input signal, where $\hat{\mathbf{u}}_s = \mathbf{u}^*$ is the estimated stator voltage obtained from the controlling signal of the linearized pulsewidth modulator in Fig. 3. As shown in Fig. 4, the vector $\hat{\mathbf{u}}_i$ of the induced voltage is integrated to form a signal $\hat{\psi}_1$. The components of this vector are subsequently limited in amplitude to the magnitude value ψ_s^* of the stator flux reference.

The trajectory of $\hat{\psi}_1$ is not circular in the presence of dc offset. Since its undisturbed radius equals ψ_s^* through the action of the stator flux controller, the offset components tend to drive the entire trajectory toward one of the $\pm\psi_s^*$ boundaries, and a clearance appears from the respective boundaries at the opposed sides. Fig. 5 shows an oscillographed example. It is seen that the offset makes the average values of the flux components $\psi_{1\alpha}$ and $\psi_{1\beta}$ nonzero. In particular, we have $(\psi_{1\alpha \min} + \psi_{1\alpha \max})/2 < 0$

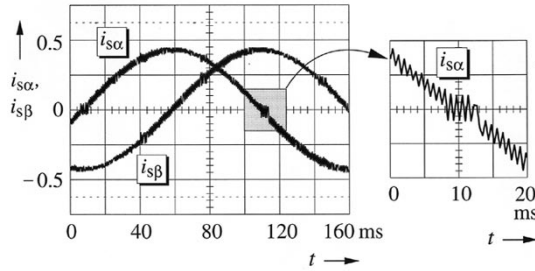


Fig. 6. Measured stator current waveforms to illustrate the zero-crossing effect.

and $(\psi_{1\beta \min} + \psi_{1\beta \max})/2 > 0$ in this example. Hence, a contribution to the offset voltage vector $\hat{\mathbf{u}}_{\text{off}}$ can be estimated from the displacement of the flux trajectory $\hat{\psi}_1$ as

$$\hat{\mathbf{u}}_{\text{off}\Delta t} = \frac{1}{\Delta t} (\hat{\psi}_{1\max} + \hat{\psi}_{1\min}) \quad (9)$$

where the maximum and minimum values in (9) are those of the respective components $\psi_{1\alpha}$ and $\psi_{1\beta}$, and Δt is the time difference between two zero crossings of $\hat{\psi}_1$ that defines a fundamental period.

Due to the nonlinear distortion of the trajectory of $\hat{\psi}_1$, the algorithm (9) is more an approximation under the conditions shown in Fig. 5. To improve on this, the signal $\hat{\mathbf{u}}_{\text{off}\Delta t}$ is low-pass filtered and fed back to the input of the integrator so as to cancel the offset component in $\hat{\mathbf{u}}_i$. The input of the integrator then tends toward zero in a quasi-steady state, which makes the estimated offset voltage vector $\hat{\mathbf{u}}_{\text{off}}$ equal the existing offset in $\hat{\mathbf{u}}_i$. The trajectory of $\hat{\psi}_1$ is exactly circular in this situation which ensures a precise tracking of the offset voltage vector.

Since offset drift is mainly a thermal effect that changes the dc offset very slowly, the response time of the offset estimator is not at all critical. It is important to note that the dynamics of stator flux estimation do not depend on the response of the offset estimator.

D. Compensation of Residual Estimation Errors

The nonideal characteristics of a PWM-inverter-fed drive system are manifold. An overview of the existing imperfections was given in Section III-A. Modeling or compensating these effects to improve the performance at zero stator frequency just uncovers new insufficiencies that went unnoticed before.

An example are the phenomena that occur when the fundamental components of the phase currents reverse their directions. The exact point of zero crossing is ill defined in the presence of switching harmonics. When a particular phase current reverses, the voltage error caused by the dead-time effect changes its sign and thus counteracts the tendency of this current to flow in the intended direction. The situation is even more complex as the superimposed switching harmonics establish repetitive changes between positive and negative current flow as illustrated in Fig. 6. Dead-time error compensation schemes fail to operate properly.

Exact voltage control by the pulsewidth modulator is impaired by an additional effect: the respective bridge arm is completely open circuited when the current is very low, and control of the corresponding phase voltage is lost. It is then the induced

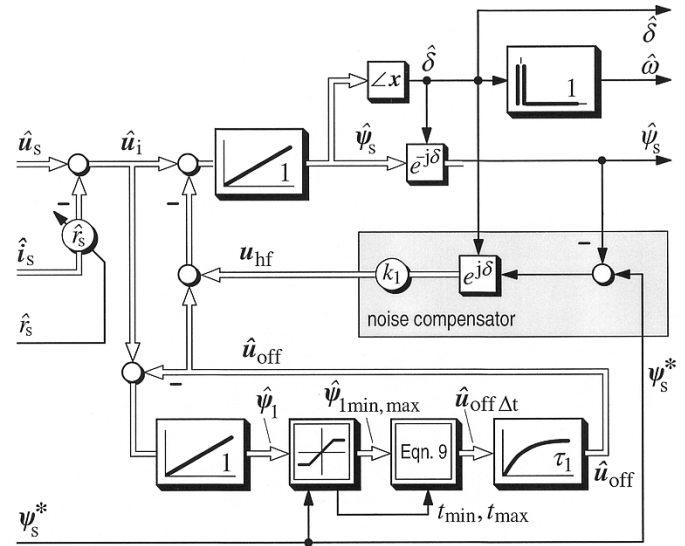


Fig. 7. Signal flow graph of a fully compensated stator flux estimator. The lower portion shows the estimator of Fig. 4.

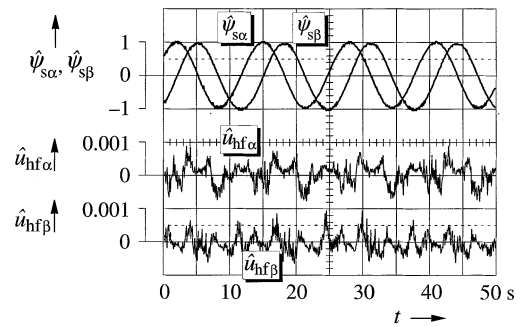


Fig. 8. Measured components of the high-frequency disturbances.

voltage of the machine that appears temporarily at this phase terminal. Estimating the exact stator voltage vector from the command value of the pulsewidth modulator becomes difficult.

The aforementioned effects produce distortions of the estimated flux vector signal that are dominated by multiple of six harmonics.

Other imperfections are discussed in Section II. It is indeed almost impossible to model or estimate all these deficiencies. However, with the dc offset accurately identified, the remaining disturbances exhibit higher, most of them much higher, frequencies than the fundamental frequency. An efficient way to minimize their impact on the estimated flux vector is adjusting the radial component of $\hat{\psi}_s$ close to its reference value ψ_s^* by fast proportional closed-loop control. This leaves the tangential component—the field angle—unaffected and thus does not interfere with the correct operation of the estimator. Moreover, a tangential error converts to a radial error after a quarter revolution of the flux vector and is then eliminated. The noise compensator shown in Fig. 7 generates the high-frequency signal \mathbf{u}_{hf} to serve this purpose. The oscillogram of Fig. 8 shows that the components of \mathbf{u}_{hf} , although very small, exhibit dominant sixth-order harmonics as predicted, and other high-frequency noise in addition.

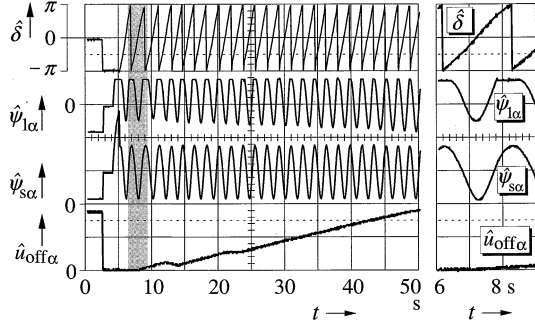


Fig. 9. Startup process with a high dc offset intentionally introduced; shaded portion enlarged on the right.

To test the dc offset estimation scheme, offset voltages of 25 mV were added to the respective inputs of the A/D converters for the α and β components of the stator current signals. The drive system was then started from a completely deenergized condition, with the speed reference set to $0.01 \approx 0.5$ Hz. The oscillogram of Fig. 9 shows that the system starts from arbitrary initial values of the flux component and field angle estimates. The machine is then energized by building an initial flux vector in the a axis. Correct estimation becomes effective at 1.5 s after starting. The high-frequency compensator first assists the stator flux estimator to establish the correct initial conditions, and then the estimated offset component $\hat{u}_{off\alpha}$ starts building up. The trace of $\hat{\psi}_{1\alpha}$ indicates that the trajectory $\hat{\psi}_1$ gradually centers in the origin. The shaded portion of this process is enlarged in the right-hand side of Fig. 9, showing that initial errors in field angle are not completely avoided in this extreme condition.

Other than assumed in [9], the noise compensator does not compensate all offset effects. It corrects only the radial flux component while leaving the tangential component unaffected. While a smooth circular flux trajectory can be also obtained in the presence of dc offset with the dc offset estimator disconnected, Fig. 10(a), the remaining phase angle error shown in Fig. 10(b) tends to destabilize the control. Fig. 10(c) shows that a tendency exists to execute oscillations.

One would rarely encounter such large offsets in a practical system. Once identified, the offset voltage vector can be stored in a nonvolatile memory to provide favorable conditions at any next start. Fig. 16 shows an example.

E. Estimation of the Stator Resistance

Correct modeling of the stator resistance is of paramount importance for sensorless control at very low speed. The method proposed here exploits the well defined relationship between the field-oriented components of the stator current at constant flux. This condition makes the stator current vector move on a defined trajectory, the *Heyland circle*, as the load varies. The location and the size of the *Heyland circle* are independent of the stator frequency. However, the value of the stator resistance does have an influence both on the diameter and the origin of the *Heyland circle*. Fig. 11 shows that, for a given value of the torque current component i_q , the field current component i_d varies as a function of r_s .

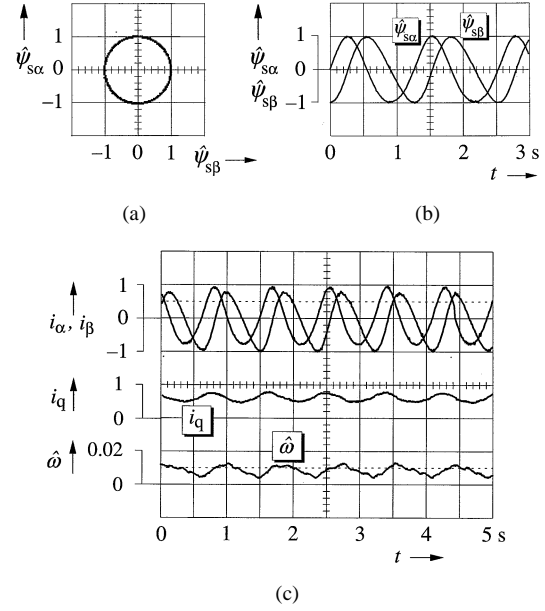


Fig. 10. Oscillograms with 250-mV dc offset intentionally introduced, showing that the noise compensator controls only the amplitude of the stator flux vector, (a). Field angle errors persist as seen in (b). (c) Circular flux vector trajectory, (b) flux vector components showing phase angle errors, and (c) oscillations in current and speed caused by field angle errors. Consequences are heavy torque and speed ripple, (c).

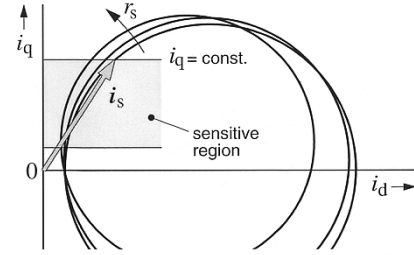


Fig. 11. Loci of the stator current vector at stator field orientation with the stator resistance as a parameter.

To exploit the effect, an analysis starts from the machine equations in a stator-flux-oriented reference frame, hence, $\psi_s = \psi_{sd} = \psi_s$. The following equations hold [12]:

$$\tau_r \frac{d\psi_s}{d\tau} + \psi_s = -\omega_r \tau_r \sigma l_s i_q + \tau_r \sigma l_s \frac{di_q}{d\tau} + l_s i_d \quad (10a)$$

$$0 = -\omega_r \tau_r (\psi_s - \sigma l_s i_d) + \tau_r \sigma l_s \frac{di_q}{d\tau} + l_s i_q \quad (10b)$$

where τ_r is the rotor time constant, l_s is the stator inductance, ω_r is the rotor (slip) frequency, and $\sigma = 1 - l_m^2/l_s l_r$ is the total leakage coefficient. Equation (10) simplifies at steady state, $d/d\tau = 0$,

$$\psi_s = -\omega_r \tau_r \sigma l_s i_q + l_s i_d \quad (11a)$$

$$l_s i_q = \omega_r \tau_r (\psi_s - \sigma l_s i_d). \quad (11b)$$

These equations permit eliminating the rotor frequency ω_r ,

$$i_d = \frac{\psi_s}{l_s + \sigma l_s} + \frac{l_s \sigma l_s}{(l_s + \sigma l_s) \psi_s} i_s^2. \quad (12)$$

The result indicates that the d -axis current has a defined magnitude at any given excitation and load, expressed by ψ_s and

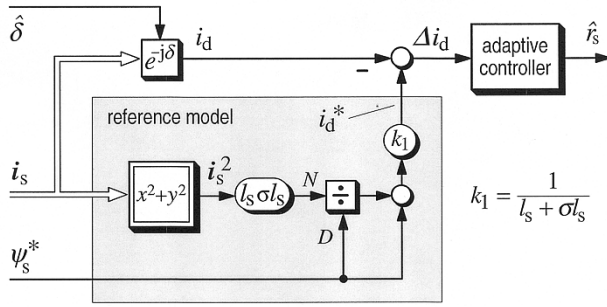


Fig. 12. Stator resistance estimation by model reference adaptive control; the adjustable model is the stator flux estimator in Fig. 7, being manipulated by the adaptive controller in the upper right. N : numerator; D : denominator.

i_s , provided that correct stator field orientation exists. Equation (12) does not depend on the stator resistance. It can therefore serve as a reference model to generate the value of \hat{r}_s in the model reference adaptive system (MRAS) shown in Fig. 12. The adjustable model is the stator flux estimator Fig. 7 by virtue of its tunable stator resistance, (2). Since the correct values of u_s and i_s have already been set in this model, any error in ψ_s is caused by an incorrect value of the modeled stator resistance. Adjusting \hat{r}_s can therefore serve to satisfy (12). The machine parameters l_s and σl_s as functions of the load are determined by self-commissioning.

The convergence of this approach is proved in the following. If a stator resistance error $\Delta r_s = \hat{r}_s - r_s$ exists, a voltage error $\Delta r_s i_s$ is created. This builds an error in the stator flux vector, which is computed from (2), observing $\dot{u}_s = u_s$ as discussed before

$$\Delta \psi_s = \hat{\psi}_s - \psi_s = \Delta r_s \int i_s d\tau. \quad (13)$$

Equation (12) is rewritten as

$$\psi_s^2 - (l_s + \sigma l_s) i_d \psi_s + l_s \sigma l_s i_s^2 = 0 \quad (14)$$

becoming nonzero in the presence of a stator resistance error

$$\hat{\psi}_s^2 - (l_s + \sigma l_s) i_d \hat{\psi}_s + l_s \sigma l_s i_s^2 = \varepsilon. \quad (15)$$

The difference between (15) and (14) is

$$(\hat{\psi}_s^2 - \psi_s^2) - (l_s + \sigma l_s) i_d \Delta \psi_s = \varepsilon \quad (16)$$

which can be written with reference to (13) as

$$\varepsilon = (\hat{\psi}_s^2 - \psi_s^2) - \Delta r_s \int i_s d\tau \cdot (l_s + \sigma l_s) i_d. \quad (17)$$

It is now assumed that undisturbed voltage and current signals are used for stator flux estimation, which the offset compensation scheme ensures. A nonzero error ε can be then only caused by a stator resistance error Δr_s . Using the approximation $\psi_s^2 - \hat{\psi}_s^2 \approx -2\psi_s \Delta \psi_s$ and referring to (13), (17) demonstrates that $\varepsilon \rightarrow 0$ if $\Delta r_s \rightarrow 0$.

Although the notation r_s is used for the resistance that is estimated by this scheme, the identified quantity is in fact $r_s + r_d$ since the differential resistance r_d of the power devices appears in series with the stator winding resistance r_s .

To test the identification scheme, the stator resistances were increased to 125% of their nominal value in a step fashion. The oscillogram of Fig. 13(a) shows the response at no load and

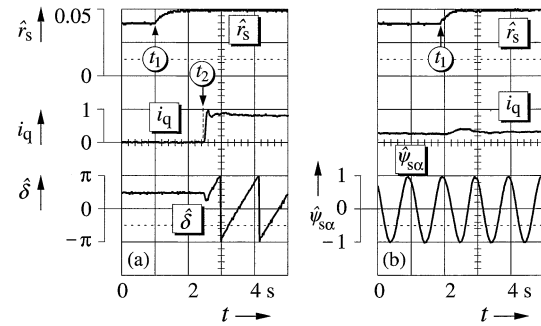


Fig. 13. Step change of the stator resistance. (a) At no load and zero stator frequency with subsequent nominal torque step. (b) At 30% rated load.

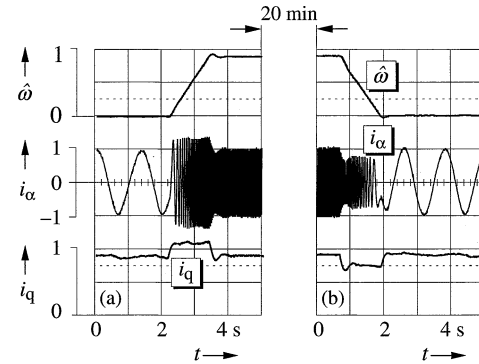


Fig. 14. Fast stator resistance identification when operating at very low speed after a transient from high speed. (a) Acceleration of the cold machine. (b) Deceleration of the heated machine.

zero stator frequency, starting at $t = t_1$. A nominal torque load step is subsequently applied at $t = t_2$, producing the desired fast and well-damped response. This indicates that the correct resistance value was identified. Fig. 13(b) shows the response to a step change of the stator resistances, applied at $t = t_1$, while operating at very low speed, $\omega = 0.01 \cong 0.5$ Hz, and 30% rated load. The estimated field angle is in error during the transient phase, as indicated by the temporary increase of i_q . The machine was not fully loaded during this experiment since a higher load than 30% rated may cause a transient instability at this very low speed. Such condition is unrealistic, though, since variations of the stator resistance are inherently owed to slow thermal effects.

The sensitivity against stator resistance mismatch reduces as the speed increases and, consequently, also the effectiveness of resistance identification schemes in general. **An accurate value of the stator resistance can only be identified if the speed is low.** It is a hard test heating a machine up at high speed with the stator resistance changing, and then returning to dynamic control at very low speed. This underlines the importance of a fast identification scheme. The response time in Fig. 13(b) is only 280 ms. Such fast reaction enables stable low-speed control following deceleration from high speed with the stator resistance initially ill identified, though a minor limiting of the speed gradient is still required. Fig. 14 shows an example.

It is an advantage of the identification method that it relies on the measured stator currents and hence is not affected by the inherent inaccuracies of stator voltage acquisition at low speed.

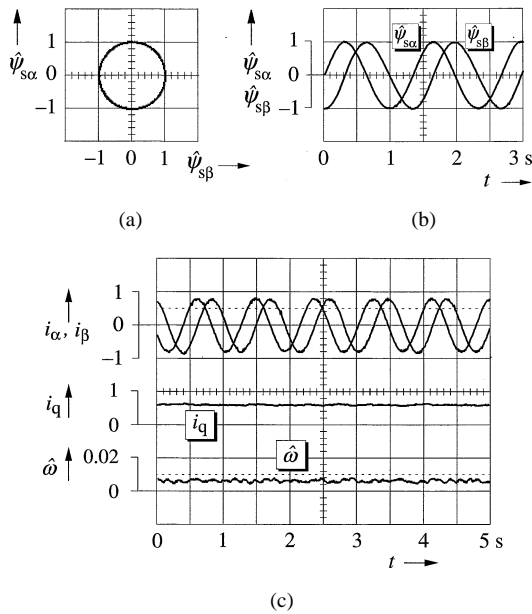


Fig. 15. Steady-state performance at low speed (33 r/min). A comparison with the waveforms in Fig. 10 demonstrates the improvement achieved by offset estimation. (a) Circular flux vector trajectory. (b) Flux vector components without phase angle error. (c) Stator current waveforms and estimated speed.

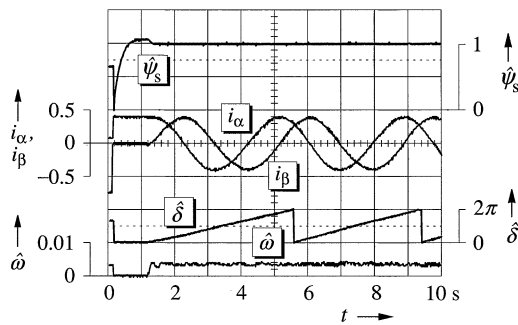


Fig. 16. Startup of the deenergized drive system for operation at 0.005 rated speed (0.25 Hz).

However, Fig. 11 shows that it does require a minimum torque current of about 15% i_{qR} to make the effect of r_s on i_d apparent, where the subscript R denotes a rated value. The method described in [9] is, therefore, preferred at light load, but its use must be inhibited at very low speed as it becomes inaccurate.

IV. SYSTEM PERFORMANCE

The effectiveness of the offset estimator is illustrated by the oscillograms of Fig. 15. The waveforms of the stator flux components in Fig. 15(b) appear perfectly sinusoidal as opposed to those in Fig. 10(b). Both oscillograms were recorded with 250-mV offset intentionally added to the current signals i_α and i_β . The stator currents are sinusoidal in Fig. 15(c), producing a constant torque as indicated by the signal i_q . The signal of the estimated speed is smoothed, although not ideally, which is owed to the low frequency of operation (0.023 rated speed, or 1.14 Hz).

The oscillogram of Fig. 16 shows a startup process of the deenergized drive system with subsequent operation at 0.005

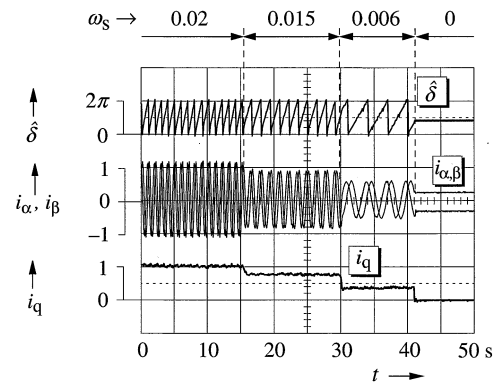


Fig. 17. Zero-speed operation with the load reducing in steps from 130% nominal torque to no load; ω_s indicated on top.

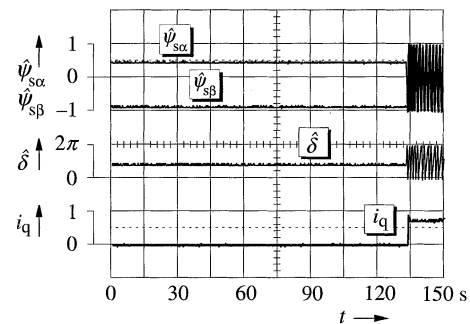


Fig. 18. Long-term zero-speed operation followed by a nominal torque step.

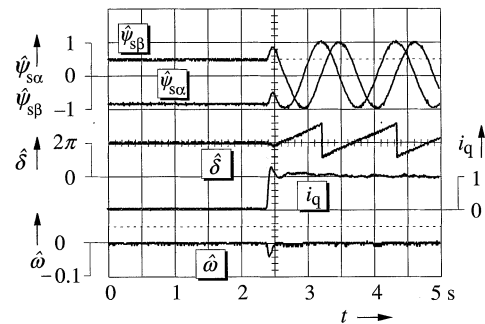


Fig. 19. Load rejection response with a 120% torque step applied at zero speed.

rated speed (0.25 Hz). The recorded variables assume arbitrary values in the very beginning while the state of the drive system is not yet fully identified. In Fig. 17, the speed reference is set to zero while the load is reduced in steps from 120% nominal torque. Stable zero stator frequency operation is finally reached at no load. Fig. 18 demonstrates that the field angle is correctly estimated without drift, even during an extended time of zero-stator-frequency operation. The subsequent response to a torque step of rated magnitude demonstrates that full dynamic controllability is maintained. The time expansion of such process with a torque step of 120% nominal magnitude applied is shown in Fig. 19. Accurate zero-speed operation is resumed after a short unavoidable transient. Finally, Fig. 20 shows the response to a negative torque step disturbance of rated magnitude applied during speed controlled operation at 0.3% rated speed. The drive operates in the regeneration mode after the step. A tendency to

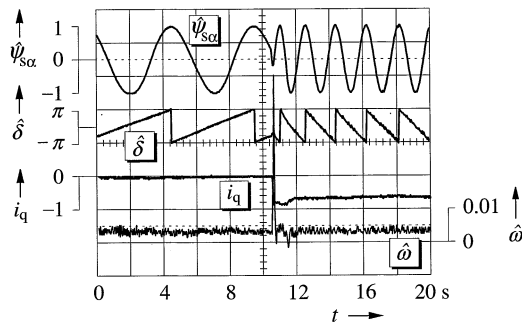


Fig. 20. Rated torque step applied at $\omega = 0.003$ with subsequent operation at regeneration.

destabilize at regeneration has been observed at this very low speed.

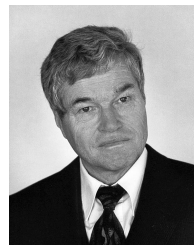
V. SUMMARY

A precise and robust sensorless control system for induction machines is based on a refined stator flux identification scheme. A dc offset voltage estimator and a noise compensator are used to generate undisturbed voltage and current signals as the inputs to the stator flux estimator. The absence of offset and drift permits using a pure integrator to derive the stator flux linkage vector from the vector of the induced voltage. The method thus eliminates all existing bandwidth restrictions for flux estimation. It enables smooth operation at very low speed and long-term stability at zero stator frequency while maintaining full dynamic controllability. Accurate dynamic torque control is achieved by a fast stator resistance estimation scheme. The correction of ill-defined resistance values accumulated in the unobservable high-speed region is demonstrated while reentering the low-speed region in a transient process.

REFERENCES

- [1] K. Rajashekara, A. Kawamura, and K. Matsuse, Eds., *Sensorless Control of AC Motors*. New York: IEEE Press, 1996.
- [2] J. Holtz, "Sensorless position control of induction motors—An emerging technology," *IEEE Trans. Ind. Electron.*, vol. 45, pp. 840–852, Dec. 1998.
- [3] M. W. Degner and R. D. Lorenz, "Using multiple saliencies for the estimation of flux, position and velocity in AC machines," *IEEE Trans. Ind. Appl.*, vol. 34, pp. 1097–1104, Sept./Oct. 1998.
- [4] N. Teske, G. M. Asher, M. Summer, and K. J. Bradley, "Suppression of saturation saliency effects for the sensorless position control induction motor drives under loaded conditions," *IEEE Trans. Ind. Appl.*, vol. 47, pp. 1142–1149, Sept./Oct. 2000.
- [5] J. Holtz and H. Pan, "Elimination of saturation effects in sensorless position controlled induction motors," presented at the IEEE-IAS Annu. Meeting, Chicago, IL, Oct. 13–18, 2002.
- [6] J. Holtz, "The representation of AC machine dynamics by complex signal flow graphs," *IEEE Trans. Ind. Electron.*, vol. 42, pp. 263–271, June 1995.
- [7] H. Kubota, Y. Kataoka, H. Ohta, and K. Matsuse, "Sensorless vector controlled induction machine drives with fast stator voltage offset compensation," presented at the IEEE-IAS Annu. Meeting, Phoenix, AZ, Oct. 1999.
- [8] J.-W. Choi and S.-K. Sul, "Inverter output voltage synthesis using novel dead time compensation," *IEEE Trans. Power Electron.*, vol. 11, pp. 221–224, Apr. 1996.
- [9] J. Holtz and J. Quan, "Sensorless vector control of induction motors at very low speed using a nonlinear inverter model and parameter identification," *IEEE Trans. Ind. Appl.*, vol. 38, pp. 1087–1095, July/Aug. 2002.

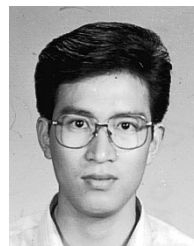
- [10] Th. Frenze, F. Hoffman, and H. G. Langer, "Speed sensorless control of traction drives—Experiences on vehicles," in *Proc. 8th Europ. Conf. Power Electronics and Applications (EPE'99)*, Lausanne, Switzerland, 1999, CD-ROM.
- [11] D.-W. Chung and S.-K. Sul, "Analysis and compensation of current measurement error in vector-controlled AC motor drives," *IEEE Trans. Ind. Appl.*, vol. 34, pp. 340–345, Mar./Apr. 1998.
- [12] J. Holtz, "Sensorless control of induction motors," *Proc. IEEE*, vol. 90, pp. 1359–1394, Aug. 2002.
- [13] J. Hu and B. Wu, "New integration algorithms for estimating motor flux over a wide speed range," *IEEE Trans. Power Electron.*, vol. 13, pp. 969–977, Sept. 1998.
- [14] M. Rodic and K. Jezernik, "An analysis of speed sensorless torque and flux controller for induction motor," in *Proc. IEEE PESC*, Galway, Ireland, 2000, CD-ROM.
- [15] I.-J. Ha and S.-H. Lee, "An online identification method for both stator and rotor resistances of induction motors without rotational transducers," *IEEE Trans. Ind. Electron.*, vol. 47, pp. 842–853, Aug. 2000.
- [16] S. Mir, E. Elbuluk, and D. S. Zinger, "PI and fuzzy estimators for tuning the stator resistance in direct torque control of induction machines," *IEEE Trans. Power Electron.*, vol. 13, pp. 279–287, Mar. 1998.
- [17] G. Guidi and H. Umida, "A sensorless induction motor drive for low speed applications using a novel stator resistance estimation method," presented at the IEEE-IAS Annu. Meeting, Phoenix, AZ, Oct. 1999.



Joachim Holtz (M'87–SM'88–F'93) graduated in 1967 and received the Ph.D. degree in 1969 from the Technical University Braunschweig, Braunschweig, Germany.

In 1969, he became an Associate Professor and, in 1971, he became a Full Professor and Head of the Control Engineering Laboratory, Indian Institute of Technology, Madras, India. In 1972, he joined the Siemens Research Laboratories, Erlangen, Germany. From 1976 to 1998, he was a Professor and Head of the Electrical Machines and Drives Laboratory, Wuppertal University, Wuppertal, Germany. He is currently a Consultant. He has authored more than 120 technical papers, including 70 refereed publications in journals. He has also authored 17 invited conference papers and ten invited papers published in journals. He is the coauthor of four books and the holder of 30 patents.

Dr. Holtz was the recipient of the IEEE Industrial Electronics Society Dr. Eugene Mittelmann Achievement Award, the IEEE Industry Applications Society Outstanding Achievement Award, the IEEE Power Electronics Society William E. Newell Field Award, the IEEE Third Millennium Medal, and the IEEE Lamme Gold Medal. He has earned seven IEEE Prize Paper Awards. He is Past Editor-in-Chief of the IEEE TRANSACTIONS ON INDUSTRIAL ELECTRONICS, a Distinguished Lecturer of the IEEE Industry Applications and IEEE Industrial Electronics Societies, a Senior AdCom Member of the IEEE Industrial Electronics Society, and member of the Static Power Converter Committee of the IEEE Industry Applications Society.



Juntao Quan was born in Jiangxi, China, in 1964. He received the B.Eng. degree from Jiangxi Polytechnic College, Nanchang University, Nanchang, China, the M.Eng. degree from Northeast-Heavy Mechanic Institute, Yanshan University, Qinhuangdao, China, and the Ph.D. degree from Wuppertal University, Wuppertal, Germany, in 1983, 1989, and 2002, respectively, all in electrical engineering.

He was an Assistant Electrical Engineer for three years at the Nanchang Bus Factory, Nanchang, China. From 1989 to 1994, he was a Lecturer at Yanshan University. During this time, he also worked on various projects for applications of power electronics. In 1995, he joined the Electrical Machines and Drives Laboratory, Wuppertal University, where he worked and studied toward the Ph.D. degree. In June 2000, he joined the Danaher Motion Group, Kollmorgen-Seidel, Duesseldorf, Germany, as an R&D Engineer. Since April 2003, he has been with Rockwell Automation AG, Luzern, Switzerland. His main interests are in the areas of adjustable-speed drives, microprocessor-embedded real-time control, power electronics applications, and advanced motion control.